
**Liquid Crystals**
Publication details, including instructions for authors and subscription information:
http://www.informaworld.com/smpp/title~content=t713926090

# Glass formation in the Gay-Berne nematic liquid crystal

A. M. Smondyrev; Robert A. Pelcovits

Online publication date: 06 August 2010

**To cite this Article** Smondyrev, A. M. and Pelcovits, Robert A.(1997) 'Glass formation in the Gay-Berne nematic liquid crystal', Liquid Crystals, 23: 2, 205 — 212
**To link to this Article: DOI:** 10.1080/026782997208451
**URL:** http://dx.doi.org/10.1080/026782997208451

LIQUID CRYSTALS, 1997, VOL. 23, NO. 2, 205–212

# Glass formation in the Gay–Berne nematic liquid crystal

by A. M. SMONDYREV and ROBERT A. PELCOVITS*
Department of Physics, Brown University, Providence, Rhode Island 02912, U.S.A.

(*Received 21 January 1997; accepted 14 February 1997*)

We present the results of molecular dynamics simulations of the Gay–Berne model of liquid crystals, supercooled from the nematic phase at constant pressure. We find a glass transition to a metastable phase with nematic order and frozen translational and orientational degrees of freedom. For fast quench rates the local structure is nematic-like, while for slower quench rates smectic order is present as well.



## 1. Introduction

The study of nematic glasses [1] is richer than the corresponding study of isotropic glasses due to the presence of orientational degrees of freedom in the former systems. Assuming that we supercool a liquid crystal starting from its nematic phase (rather than the isotropic phase) we expect a nematic glass to have long range orientational order like an equilibrated nematic as well as frozen density and director fluctuations. Orientationally this glassy phase is similar to a mixed magnetic phase where both ferromagnetic and vector spin glass order coexist [2]. However, unlike a spin glass the nematic glass is a nonequilibrium phase of matter and the molecular translational degrees of freedom freeze as well at the glass transition.

In this paper we study the formation of a nematic glass using molecular dynamics (MD). We model the liquid crystal using the Gay–Berne (GB) potential [3] which is an anisotropic Lennard–Jones potential. Previous molecular dynamics studies have indicated that the Gay–Berne potential exhibits a rich phase diagram [4–6] and the principal dynamical features [7–10] of real liquid crystals. The GB potential is given by

$$U(\hat{\mathbf{u}}_1, \hat{\mathbf{u}}_2, \mathbf{r}) = 4\varepsilon(\hat{\mathbf{u}}_1, \hat{\mathbf{u}}_2, \mathbf{r}) \times \left[ \left\{ \frac{\sigma_o}{r - \sigma(\hat{\mathbf{u}}_1, \hat{\mathbf{u}}_2, \mathbf{r}) + \sigma_o} \right\}^{12} - \left\{ \frac{\sigma_o}{r - \sigma(\hat{\mathbf{u}}_1, \hat{\mathbf{u}}_2, \mathbf{r}) + \sigma_o} \right\}^{6} \right] \tag{1}$$

where $\hat{\mathbf{u}}_1, \hat{\mathbf{u}}_2$ are unit vectors giving the orientations of the two molecules separated by the position vector $\mathbf{r}$. The parameters $\varepsilon(\hat{\mathbf{u}}_1, \hat{\mathbf{u}}_2, \mathbf{r})$ and $\sigma(\hat{\mathbf{u}}_1, \hat{\mathbf{u}}_2, \mathbf{r})$ are orientation dependent and give the well depth and the intermolecular separation where $U = 0$, respectively. The well depth is written as

$$\varepsilon(\hat{\mathbf{u}}_1, \hat{\mathbf{u}}_2, \mathbf{r}) = \varepsilon_o \varepsilon^{\nu}(\hat{\mathbf{u}}_1, \hat{\mathbf{u}}_2) \varepsilon'^{\mu}(\hat{\mathbf{u}}_1, \hat{\mathbf{u}}_2, \mathbf{r}) \tag{2}$$

where

$$\varepsilon(\hat{\mathbf{u}}_1, \hat{\mathbf{u}}_2) = (1 - \chi^2(\hat{\mathbf{u}}_1, \hat{\mathbf{u}}_2)^{-1/2} \tag{3}$$

and

$$\varepsilon'(\hat{\mathbf{u}}_1, \hat{\mathbf{u}}_2, \hat{\mathbf{r}}) = 1 - \frac{\chi}{2} \left\{ \frac{(\hat{\mathbf{r}}\ \mathbf{u}_1 + \hat{\mathbf{r}}\ \mathbf{u}_2)^2}{1 + \chi'(\mathbf{u}_1\ \mathbf{u}_2)} + \frac{(\hat{\mathbf{r}}\ \mathbf{u}_1 - \hat{\mathbf{r}}\ \mathbf{u}_2)^2}{1 - \chi'(\mathbf{u}_1\ \mathbf{u}_2)} \right\}. \tag{4}$$

The range parameter $\sigma(\mathbf{u}_1, \hat{\mathbf{u}}_2, \mathbf{r})$ is given by

$$\sigma(\hat{\mathbf{u}}_1, \hat{\mathbf{u}}_2, \hat{\mathbf{r}}) = \sigma_o \left\{ 1 - \frac{\chi}{2} \left\{ \frac{(\hat{\mathbf{r}}\ \mathbf{u}_1 + \hat{\mathbf{r}}\ \mathbf{u}_2)^2}{1 + \chi(\mathbf{u}_1\ \mathbf{u}_2)} + \frac{(\hat{\mathbf{r}}\ \mathbf{u}_1 - \hat{\mathbf{r}}\ \mathbf{u}_2)^2}{1 - \chi(\mathbf{u}_1\ \mathbf{u}_2)} \right\} \right\}^{-1/2}. \tag{5}$$

The shape anisotropy parameter $\chi$ is given by

$$\chi = \{(\sigma_e/\sigma_s)^2 - 1\}/\{(\sigma_e/\sigma_s)^2 + 1\} \tag{6}$$

where $\sigma_e$ and $\sigma_s$ are the separation of end-to-end and side-by-side molecules respectively. The parameter $\chi'$ is given by

$$\chi' = \{1 - (\varepsilon_e/\varepsilon_s)^{1/\mu}\}/\{1 + (\varepsilon_e/\varepsilon_s)^{1/\mu}\}. \tag{7}$$

The ratio of the well depths for end-to-end and side-by-side configurations is $\varepsilon_e/\varepsilon_s$.

We investigated glass formation in the Gay–Berne fluid using a constant-pressure, constant-temperature MD method [11], which allows the volume to change as a function of the temperature and pressure of the system. The edges of the cell were allowed to vary independently, but the orthogonal shape was maintained. We simulated a system of $N = 864$ particles. We chose $\sigma_e/\sigma_s = 3$, $\varepsilon_e/\varepsilon_s = 5$, and $\nu = 1$ and $\mu = 2$ as in the original work of Gay and Berne. The moment

*Author for correspondence.

0267–8292/97 $12·00 

of inertia was chosen to be $4m\sigma_0^2$, as in [10]. We used periodic boundary conditions, and cut-off and smoothed the potential at $3{\cdot}8\sigma_0$. The equation of motion were solved using the leap-frog algorithm with an integration time-step $\Delta t^* = 0{\cdot}001$ in dimensionless units ($\Delta t^* = \Delta t(m\sigma_0^2/\varepsilon_0)^{-1/2}$, where $m$ is the mass of a molecule). In order to study glass formation (an inherently non-equilibrium phenomenon) in this system we first studied the formation of equilibrium phases when the system is allowed to equilibrate for a long time (typically tens of thousands of iterations) at each temperature. To the best of our knowledge, this is the first time a constant-pressure, constant-temperature MD method has been applied to study the Gay–Berne mesogen, though constant-pressure Monte Carlo investigations have previously been carried out [12]. The results of the equilibrium runs are presented in the next section. In § 3 we consider the supercooling runs where the system was started in the nematic phase and then cooled in a rapid stepwise fashion to low temperatures.



## 2. Equilibrium phases

The initial configuration was generated by locating nearly parallel molecules at the sites of an fcc lattice, with the average director parallel to the long diagonal of the cubic MD cell. The dimensionless temperature $T^*(\equiv k_B T/\varepsilon_0) = 3{\cdot}0$ and pressure $P^*(\equiv P\sigma_0^3/\varepsilon_0) = 5{\cdot}8$† were chosen. We carried out a long run (20 000 iterations) which reduced the nematic order parameter to 0·1 and disordered the system translationally. The temperature was then reduced in a sequential fashion allowing the system to relax at each temperature for 20 000–80 000 iterations. Figures 1–3 show the order parameter, potential energy and MD cell dimensions respectively as functions of temperature.

Above $T^* = 1{\cdot}2$ the system is disordered, the MD cell is still cubic and fluctuations of the director are large. At $T^* = 1{\cdot}2$ the value of the order parameter rises rapidly to $S = 0{\cdot}66$, and a break is observed in the potential energy curve which suggests that the isotropic–nematic transition has occurred. At this point the director becomes parallel to one of the edges of the cell and its fluctuations are negligible. Significant changes also occur in the shape of the MD cell. The dimension parallel to director becomes noticeably larger than the other two. As the system is cooled further down to $T^* = 1{\cdot}0$, the difference between cell dimensions increases and the order parameter rises to $S = 0{\cdot}844$. Below $T^* = 1{\cdot}0$ another break in order parameter and potential energy curves occurs suggesting that another phase transition has taken place. The length of the largest edge of the cell reaches a maximum at $T^* = 0{\cdot}9$ and then decreases slowly as the temperature decreases. The nature of the new phase becomes clear by comparing parallel, perpendicular (relative to the director) and orientationally-averaged pair distribution functions at $T^* = 1{\cdot}1$ (see figure 4) and $T^* = 0{\cdot}9$ (see figure 5).

Figure 4 exhibits liquid-like behaviour which is typical of a nematic phase. The parallel distribution function in figure 5 exhibits strong periodic structure with relatively narrow peaks, indicating a layered structure, with the layer normal parallel to the director (i.e. a smectic A phase†). The separation between the layers is $2{\cdot}5\sigma_0$

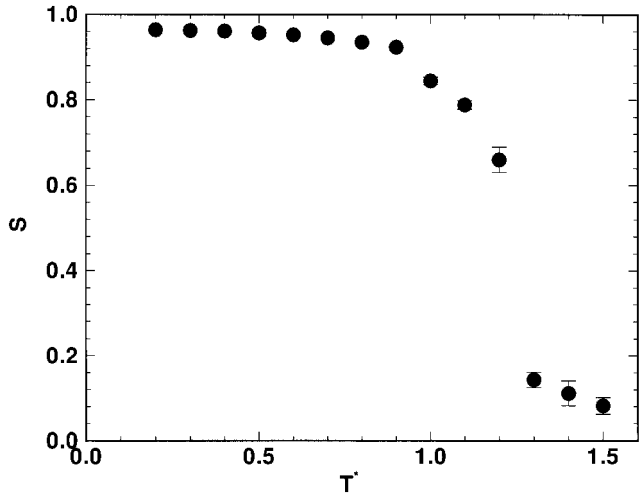


Figure 1. The nematic order parameter as a function of temperature (in dimensionless units) in thermal equilibrium.

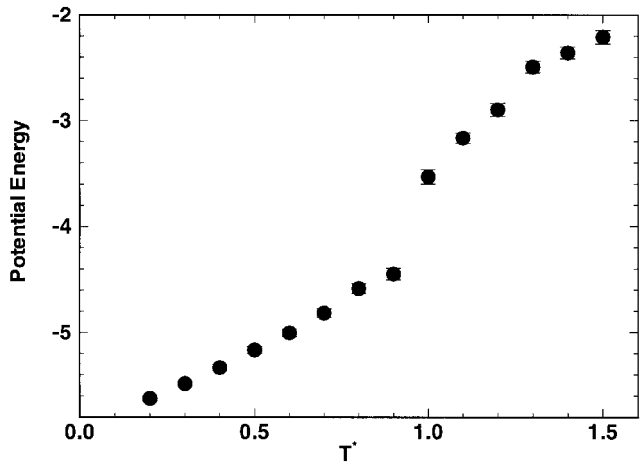


Figure 2. The potential energy in dimensionless units as a function of temperature (in dimensionless units) in thermal equilibrium.

† At this dimensionless pressure the Gay–Berne fluid has isotropic, nematic, smectic and crystalline phases; see [4].

† We see no evidence of hexatic order in the layers leading us to believe that this phase is smectic A. However, other studies (see ref. [4]) have found evidence of hexatic order, in which case the phase is labelled smectic B.

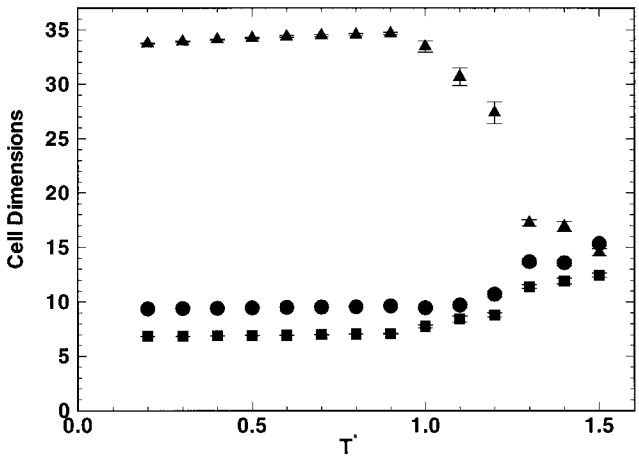


Figure 3. The dimensions of the MD cell as a function of temperature (in dimensionless units). The dimensions of the cell along the $x$, $y$, and $z$ axes are denoted by squares, triangles and circles respectively. Nematic order develops along the $y$ axis.

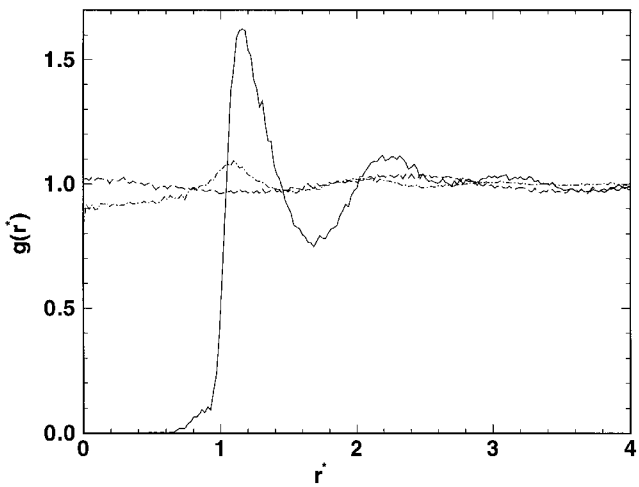


Figure 4. The pair distribution function versus distance in dimensionless units ($r^* \equiv r/\sigma_o$) for the nematic phase at $T^* = 1{\cdot}1$. The solid curve is the orientationally averaged function. The dashed curve is the distribution function parallel to the director plotted against distance parallel to the director. The dashed–dotted curve is the distribution function perpendicular to the director (averaged over the parallel direction) plotted against distance perpendicular to the director.

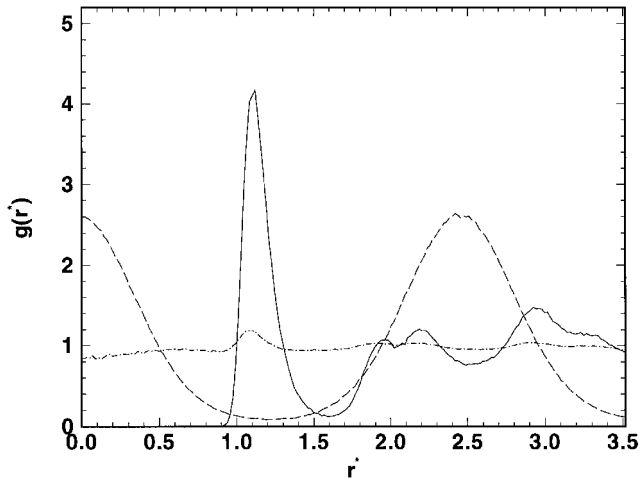


Figure 5. The pair distribution function versus distance in dimensionless units ($r^* \equiv r/\sigma_o$) for the smectic phase at $T^* = 0{\cdot}9$. The line style of the three curves is as in figure 4. The peaks in the parallel distribution function indicate that smectic layers have formed. Within the layers the structure is still liquid-like.

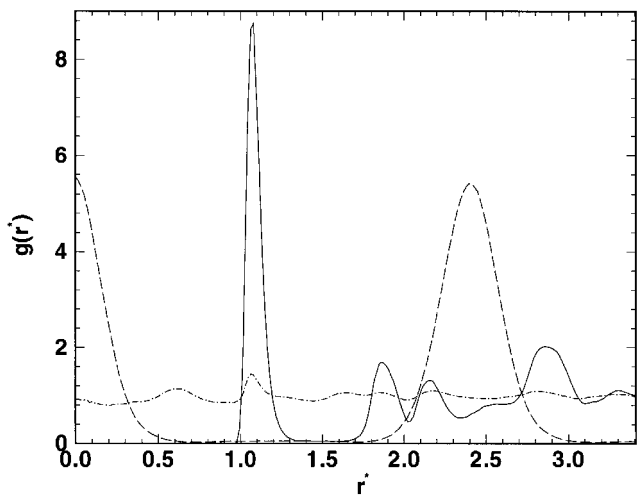


Figure 6. The pair distribution function versus distance in dimensionless units ($r^* \equiv r/\sigma_o$) for the crystalline phase at $T^* = 0{\cdot}2$. The line style of the three curves is as in figure 4. The peaks in the parallel distribution function are sharper than the same peaks in the smectic phase. The translational ordering within the layers is indicated by the sharper peaks in the perpendicular and rotationally averaged distribution functions, and the presence of a new peak near $r^* = 0{\cdot}5$ in the perpendicular function.

which suggests interpenetration of adjacent layers due primarily to the ellipsoidal shape of the molecules. At even lower temperatures the system crystallizes. The distribution functions at $T^* = 0{\cdot}2$ are shown in figure 6. The stronger separation between the double peaks of the orientationally averaged distribution function at $r^*(\equiv r/\sigma_0) = 2{\cdot}0$ shows the increased ordering within the layers, while the first peak at $r^* = 0{\cdot}5$ in the perpendicular distribution function shows the correlation of molecular positions in adjacent layers. Further proof of crystallization can be obtained from dynamical properties of the system, characterized by the translational diffusion coefficients and orientational relaxation times. Diffusion coefficients parallel and perpendicular to the director are evaluated from mean-squared displacements as

follows:

$$D_{\parallel} = \lim_{t\to\infty} \frac{1}{6t}\langle (r_{\parallel}(t+t_0) - r_{\parallel}(t_0))^2\rangle \tag{8}$$

$$D_{\perp} = \lim_{t\to\infty} \frac{1}{6t}\langle (\mathbf{r}_{\perp}(t+t_0) - \mathbf{r}_{\perp}(t_0))^2\rangle. \tag{9}$$

In the nematic phase the ratio of the two diffusion constants $D_{\parallel}/D_{\perp}$ is approximately 4. In the smectic phase perpendicular diffusion becomes dominant and the ratio of the diffusion constants becomes approximately 0·7 (see table 1). Below $T^* = 0{\cdot}7$ the parallel diffusion constant becomes extremely small, about 10 times smaller than in the smectic phase. Molecular motion perpendicular to the director is dominated by random fluctuations about equilibrium positions, and the diffusion coefficient cannot be determined. This indicates that a crystalline phase has formed.

Finally, to explore the intralayer structure, we examined snapshots of the three layers located in the middle of the cell. At $T^* = 0{\cdot}9$, corresponding to a smectic phase (see figure 7) there is neither translational nor bond-orientational order within the layers. At $T^* = 0{\cdot}2$ (see figure 8) the system shows both translational order and bond-orientational order. The molecular positions in different layers are noticeably correlated. The honeycomb lattice in the middle layer is shifted with respect to the two outer lattices, yielding a hexagonal close-packed structure and freezing of intralayer diffusion.

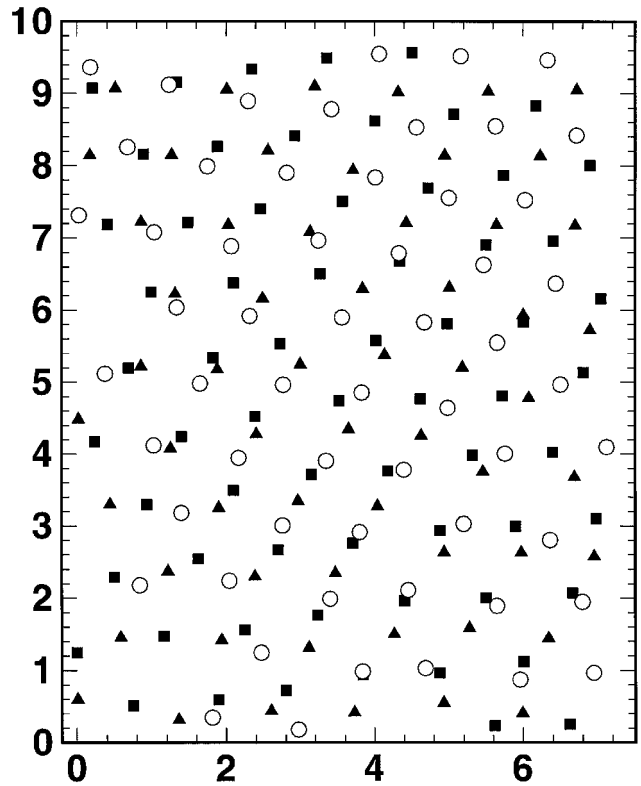


Figure 7. The $x$–$y$ locations of the molecules in the three innermost smectic layers of the MD cell (there are fifteen layers in total) for the smectic phase at $T^* = 0{\cdot}9$. The MD cell is viewed from above, and the director is perpendicular to the figure. The units are dimensionless length. The triangles correspond to molecules in the middle layer of the three layers shown, while the boxes and circles correspond to the two layers which flank the middle one. Notice the absence of long range bond orientational and translational order. Locally, the centres of mass of the molecules form imperfect hexagons.

### 3. Glass formation

The initial configuration was chosen in the nematic phase at the dimensionless temperature $T^* = 1{\cdot}2$ and pressure $P^* = 5{\cdot}8$. The nematic order parameter at this point in the phase diagram is $S = 0{\cdot}75$. The temperature was then reduced in a sequential fashion allowing the system to relax at each temperature for a number of time steps depending on the quench rate. The quench rate is defined by the ratio of the change in dimensionless temperature to the number of timesteps between two succeeding temperature reductions. Our discussion will focus primarily on simulations where the temperature was lowered in decrements of $\Delta T^* = 0{\cdot}1$ every 100 iterations, corresponding in real units to a quench rate approximately equal to $10^{13}\,\mathrm{K\,s^{-1}}$. Rates faster and slower than this one will be discussed at the end of this section. After the system was cooled to its final temperature, it was allowed to anneal and various structural and dynamical properties were measured. Figure 9 shows the potential energy as a function of the annealing time at four different final temperatures. The breaks in the curves corresponding to temperatures $T^* = 0{\cdot}4$ and

Table 1. Diffusion constants parallel and perpendicular to the director for the system in equilibrium.

| | $D_{\parallel}$ | $D_{\perp}$ | $D_{\parallel}/D_{\perp}$ |
|---|---|---|---|
| Nematic, $T^* = 1{\cdot}2$ | $0{\cdot}168 \pm 0{\cdot}005$ | $0{\cdot}0384 \pm 0{\cdot}0003$ | 4·38 |
| Nematic, $T^* = 1{\cdot}1$ | $0{\cdot}092 \pm 0{\cdot}001$ | $0{\cdot}0215 \pm 0{\cdot}0001$ | 4·27 |
| Nematic, $T^* = 1{\cdot}0$ | $0{\cdot}049 \pm 0{\cdot}001$ | $0{\cdot}0115 \pm 0{\cdot}0001$ | 4·23 |
| Smectic, $T^* = 0{\cdot}9$ | $0{\cdot}00101 \pm 0{\cdot}00003$ | $0{\cdot}00136 \pm 0{\cdot}0001$ | 0·787 |
| Smectic, $T^* = 0{\cdot}8$ | $0{\cdot}00049 \pm 6 \times 10^{-6}$ | $0{\cdot}00069 \pm 1{\cdot}9 \times 10^{-5}$ | 0·711 |

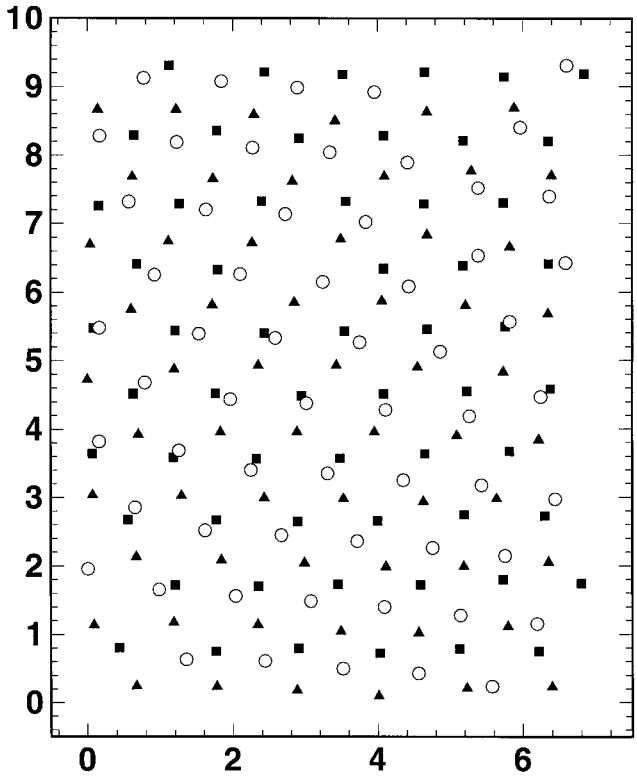


Figure 8. The $x$–$y$ locations of the molecules in the three innermost layers of the MD cell (there are fifteen layers in total) for the crystalline phase at $T^* = 0{\cdot}2$. The notation used is the same as in figure 7. Each layer forms a nearly perfect honeycomb lattice. Near the centre of the cell a hexagonal close-packed structure is evident.



$T^* = 0{\cdot}5$ suggest that crystallization may have occurred. Further proof of crystallization can be found by examining pair distribution functions after the breaks take place. Parallel, perpendicular (relative to the director) and orientationally-averaged pair distribution functions at $T^* = 0{\cdot}4$ obtained after an annealing run of 120 000 iterations and averaged over the subsequent 120 000 iterations exhibit the principal features of the distribution functions for the crystalline phase in thermal equilibrium at $T = 0{\cdot}2$. The plots of the pair distribution functions obtained after quenching to a final temperature of $T = 0{\cdot}4$ are practically indistinguishable from those shown in figure 6. However, quenches to temperatures $T^* = 0{\cdot}3$ and below yield a different picture even after annealing. The nematic order parameter reaches a plateau at long times (see figure 10), with average values lower than the corresponding values in the equilibrium phase at the same temperature ($S = 0{\cdot}878$, $0{\cdot}920$ in the quenched system, $S = 0{\cdot}964$, $0{\cdot}962$ in the equilibrium system for $T^* = 0{\cdot}2$, $0{\cdot}3$, respectively). The pair distribution functions for a system quenched to $T^* = 0{\cdot}2$ and then annealed for 120 000 iterations are shown in figure 11. There is no smectic layer formation and no

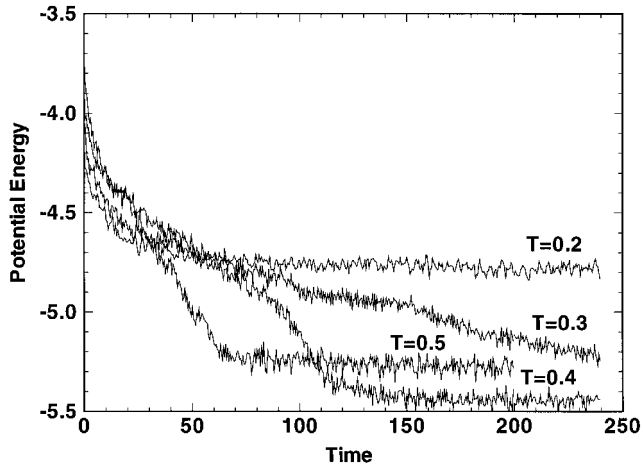


Figure 9. The potential energy in dimensionless units as a function of annealing time (in dimensionless units) for a Gay–Berne fluid quenched from $T^* = 1{\cdot}2$ to the temperatures indicated. The quench rate corresponded to a reduction in temperature of $0{\cdot}1$ every 100 iterations. The quench was completed at time equals 0 in this figure. Note the absence of a break in the curves corresponding to the temperatures $T^* = 0{\cdot}2$ and $0{\cdot}3$, unlike the two higher temperatures. The system at $T^* = 0{\cdot}3$ is probably very close to glass transition temperature $T_g$. The potential energy at this latter temperature does not exhibit the plateau seen at $T = 0{\cdot}2$. But the system relaxes to equilibrium much slower than the systems at higher temperatures, so that during the time interval considered it can be identified as a glass.

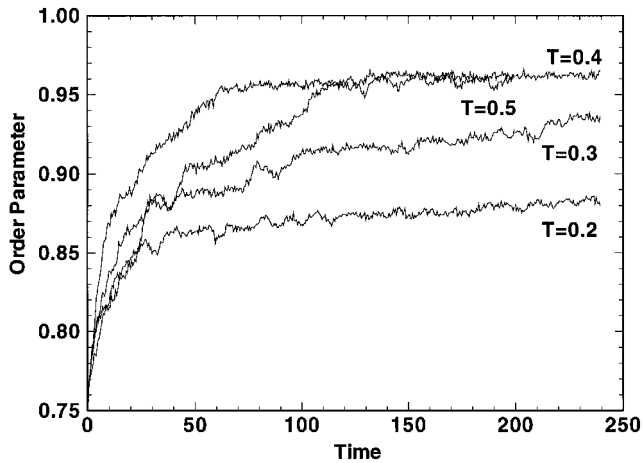


Figure 10. The nematic order parameter as a function of annealing time for quenches to the temperatures indicated. The quench rate is the same as in figure 9. Note the lower value of the order parameter for the lowest of the three temperatures shown.

translational order perpendicular to the director, i.e. structurally the quenched system is nematic-like.

We now show that the system is frozen in this nematic state both translationally and orientationally. The dynamical properties of the system are characterized by

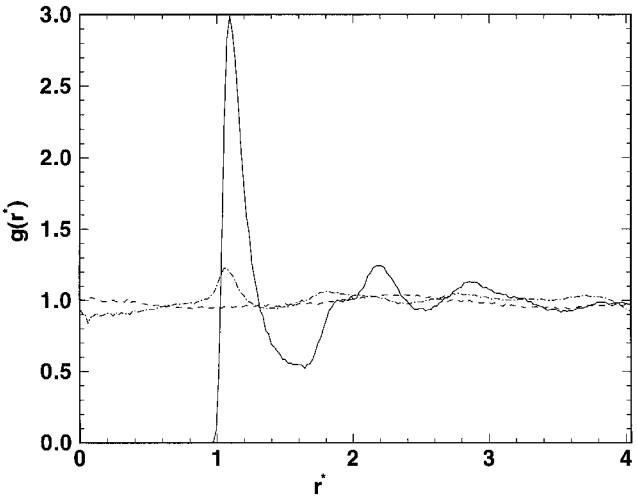


Figure 11. The pair distribution function versus distance in dimensionless units after a quench to $T^* = 0{\cdot}2$ with the same quench rate as in the previous figures. The distribution functions were evaluated after an annealing time of 120 000 iterations, and averaged over the subsequent 120 000 iterations. The line style of the three curves is as in figure 4. Note the absence of smectic order in the parallel distribution function (the dashed curve), and the absence of two well-formed subsidiary peaks in the orientationally-averaged distribution function (the solid curve). Compare with figure 6.

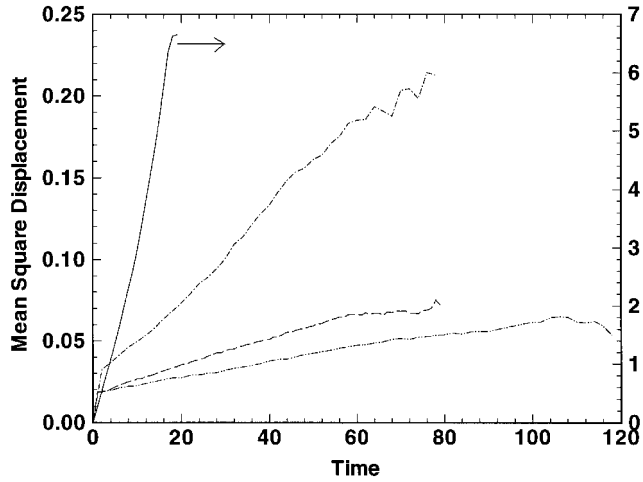


Figure 12. The mean square displacement in the direction parallel to the director in the glassy and equilibrium nematic phases. The dashed–dotted, dashed and dashed–double-dotted curves are the mean square displacements for the 'fast' quench (corresponding to a reduction in temperature of 0·1 every 100 iterations) to $T^* = 0{\cdot}3$, for the 'slow' quench (corresponding to a temperature reduction of $\Delta T^* = 0{\cdot}1$ every 1000 iteractions) to $T^* = 0{\cdot}2$, and for the 'fast' quench to $T^* = 0{\cdot}2$, respectively. The mean square displacement for the nematic in thermal equilibrium at $T = 1{\cdot}2$ is shown as a solid curve with the ordinates appearing on the right-hand axis.



the translational diffusion coefficients (equations (8) and (9)) and orientational relaxation times. Plots of mean square displacements perpendicular and parallel to the director are shown in figures 12 and 13 in the glassy phase. Their behaviour differs from that in the crystalline phase at the same temperature (figure 14). The mean square displacement parallel to the director in the glassy phase is a straight line with a nonzero slope, which increases with temperature, in contrast to the plateau seen in the crystalline phase. As the system crystallizes slow layer formation is responsible for enhanced diffusion parallel to the director. Mean square displacements perpendicular to the director in the glassy phase exhibit both crystalline and liquid-like features. The oscillations are typical of a crystalline phase, while the upward trend is a signature of a liquid phase. The slope of the upward trend changes as a function of temperature and allows us to estimate the perpendicular diffusion constant in the glassy phase. Both diffusion constants in the glassy phase are very small, about 100–1000 times smaller than corresponding values in the nematic phase which are of order 0·1 in dimensionless units. The ratio of the two diffusion constants $D_\parallel/D_\perp$ is approximately 4 in the glass phase, comparable to values in the nematic phase, and very different from the equilibrium values in the smectic and crystalline phases where the ratio is less than one and approximately equal to one, respectively.

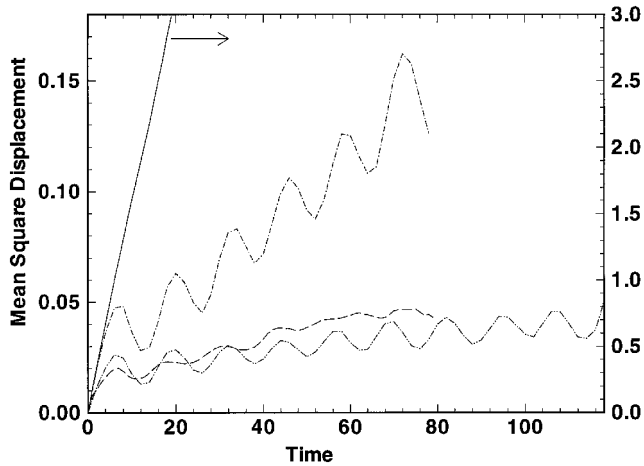


Figure 13. The mean square displacement in a direction perpendicular to the director in the glassy and equilibrium nematic phases. The notation used is the same as in figure 12.

To show that the system freezes orientationally we use the spin-glass analogy and compute an Edwards–Anderson type [13] of correlation function

$$C(t) = \frac{1}{N}\sum_{i=1}^{N}\{\langle \mathbf{u}_i(t+t_0)\mathbf{u}_i(t_0)\rangle - \langle \mathbf{u}_i(t+t_0)\rangle\langle \mathbf{u}_i(t_0)\rangle\}. \quad (10)$$

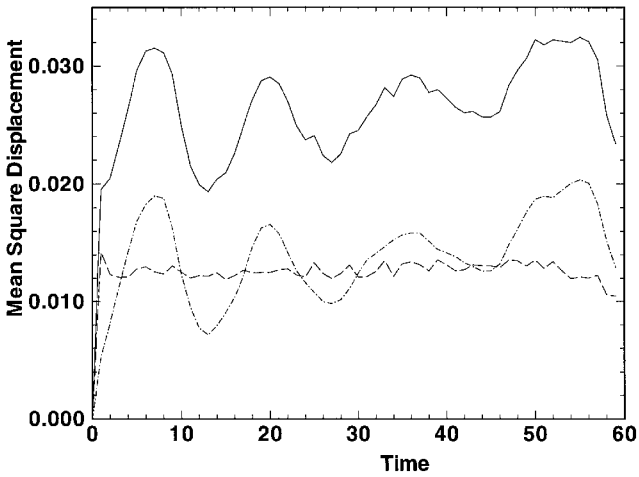


Figure 14. The mean square displacement for the crystalline phase at $T = 0{\cdot}2$. The solid, dashed and dashed–dotted curves are the mean square displacements orientationally averaged, parallel to the director and perpendicular to the director, respectively.

Logarithmic plots of correlation function $C(t)$ for different temperatures in the glassy phase and in the nematic phase are shown in figure 15. The orientational relaxation time is given by the slope of the logarithmic plot of $C(t)$ versus time $t$ and is approximately 2 orders of magnitude larger in the glass phase than in the nematic phase, as shown in table 2. Thus, our evidence suggests that a glass phase has formed at this temperature with simultaneous freezing of translational and orientational degrees of freedom.

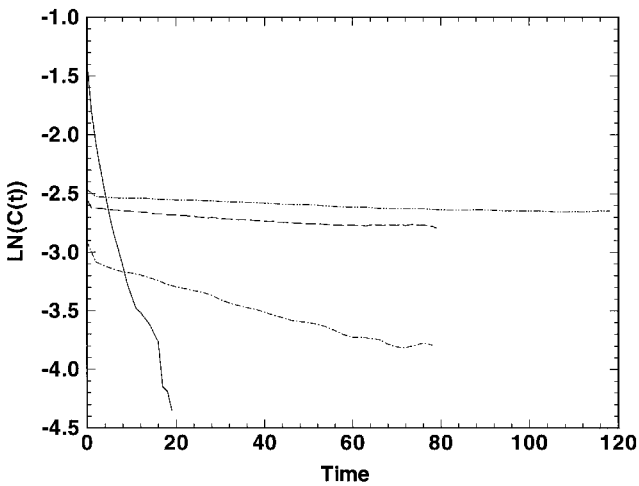


Figure 15. Logarithmic plots of the Edwards–Anderson type of correlation function $C(t)$, equation (10), in the glassy and nematic phases. The dashed–dotted, dashed, dashed–double-dotted and solid curves are data for the 'fast' quench (corresponding to a reduction in temperature of 0·1 every 100 iterations) to $T^* = 0{\cdot}3$, for the 'slow' quench (corresponding to a temperature reduction of $\Delta T^* = 0{\cdot}1$ every 1000 iterations) to $T^* = 0{\cdot}2$ for the 'fast' quench to $T^* = 0{\cdot}2$, and for the nematic in thermal equilibrium at $T = 1{\cdot}2$, respectively.

Table 2. The orientational relaxation time constant $\tau$ (defined as the slope of the logarithmic plot of $C(t)$ versus $t$ in figure 15) and the nematic order parameter $S$ at several representative temperatures for a nematic in thermal equilibrium and a glass quenched at two different rates. The fast quench rate corresponds to a temperature reduction of 0·1 every 100 iterations and the slow rate to the same reduction every 1000 iterations. The glass formed at the faster quench rate has less nematic order and significantly longer relaxation times.

| | $\tau$ | $S$ |
|---|---|---|
| Nematic, $T^* = 1{\cdot}0$ | $3{\cdot}09 \pm 0{\cdot}11$ | $0{\cdot}83 \pm 0{\cdot}01$ |
| Nematic, $T^* = 1{\cdot}1$ | $2{\cdot}72 \pm 0{\cdot}10$ | $0{\cdot}78 \pm 0{\cdot}04$ |
| Nematic, $T^* = 1{\cdot}2$ | $3{\cdot}08 \pm 0{\cdot}05$ | $0{\cdot}71 \pm 0{\cdot}04$ |
| Slow quench, $T^* = 0{\cdot}2$ | $185{\cdot}0 \pm 2{\cdot}5$ | $0{\cdot}926 \pm 0{\cdot}005$ |
| Slow quench, $T^* = 0{\cdot}3$ | $164{\cdot}3 \pm 2{\cdot}9$ | $0{\cdot}906 \pm 0{\cdot}005$ |
| Slow quench, $T^* = 0{\cdot}4$ | $14{\cdot}2 \pm 0{\cdot}2$ | $0{\cdot}927 \pm 0{\cdot}03$ |
| Fast quench, $T^* = 0{\cdot}2$ | $261{\cdot}1 \pm 8{\cdot}5$ | $0{\cdot}819 \pm 0{\cdot}007$ |
| Fast qeunch, $T^* = 0{\cdot}5$ | $243{\cdot}3 \pm 12{\cdot}6$ | $0{\cdot}804 \pm 0{\cdot}007$ |
| Fast quench, $T^* = 0{\cdot}4$ | $35{\cdot}8 \pm 1{\cdot}9$ | $0{\cdot}958 \pm 0{\cdot}004$ |

We have also considered the effects of different quench rates. If we quench the system instantaneously from $T^* = 1{\cdot}2$ to $T^* = 0{\cdot}2$ we obtain a glassy phase, qualitatively similar in structure to the one described above. However, if the glass is then annealed for several thousand time steps crystallization occurs, demonstrating that the glass becomes more unstable with increasing cooling rate, as seen in simulations of isotropic Lennard–Jones systems [14]. On the other hand, with a 'slow' cooling rate corresponding to a temperature reduction of $\Delta T^* = 0{\cdot}1$ every 1000 iterations we find a stable glassy phase. The lower quench yields a different structure than the one shown in figure 11 because of the smectic phase that intervenes between the nematic and crystalline phases under equilibrium conditions. At the slower cooling rate the system starts to form layers typical of the smectic phase, but does not crystallize. There are no correlations between the different layers and order within the layers is not perfect. These effects can be seen in figure 16 where we show the positions of the molecules in three adjacent layers of the MD cell when viewed from above for the 'slowly' quenched system at $T^* = 0{\cdot}2$. Figure 8 shows a similar view in a system which is allowed to reach thermal equilibrium at the same temperature and a crystalline phase is formed.

We have also examined the interplay between the freezing of the translational and orientational degrees of freedom. We conducted a simulation where we began in the nematic phase, but set the mass of the molecules to infinity, while maintaining the original, finite value of the moment of inertia. After a brief span of time where the molecules moved ballistically, we found that the

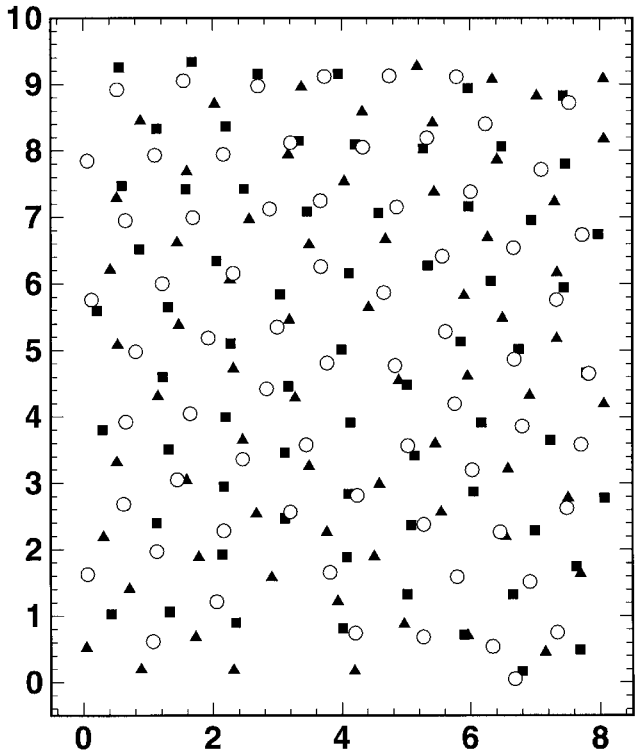


Figure 16. The $x$–$y$ locations of the molecules in the three innermost smectic layers of the MD cell (there are fifteen layers in total) for a system quenched to $T^* = 0{\cdot}2$ at the 'slow' cooling rate and then annealed for 200 000 iterations. The units are dimensionless length. The triangles correspond to molecules in the middle layer of the three layers shown. The boxes and circles correspond to the two layers which flank the middle one. Note the absence of correlations in molecular positions between layers, and decreasing hexagonal order within each layer. Compare with figure 8 which shows a system at the same temperature in thermal equilibrium and with figure 7 which shows a system in smectic phase in equilibrium at a higher temperature.



system froze orientationally, without the need to further quench the temperature. Conversely, when we set the moment of inertia to infinity but kept the mass finite we found that the diffusion constants were reduced to about one-tenth of their values in the nematic phase. While the translational degrees of freedom were sluggish, the system was not in a glassy state at this initial temperature. These two tests lead us to speculate that it is the freezing of the translational degrees of freedom which is primarily responsible for the glass transition. Once the translational degrees of freedom have frozen the orientational degrees of freedom follow suit.

## 4. Conclusions

We have carried out MD simulations on the Gay–Berne model of liquid crystals at constant temperature and pressure. Our focus has been on simulations where the system is quenched in a stepwise fashion from a temperature in the nematic phase to a temperature where a crystalline phase would form in equilibrium. For low enough final temperatures we find that the system forms a glassy phase. This phase has the structure of a frozen nematic (or a frozen smectic if the quench rate is lowered), where both translational and orientational degrees of freedom are frozen. The freezing is characterized by diffusion constants which are orders of magnitude smaller than the corresponding ones in the nematic phase, and an orientational relaxation time which is two orders of magnitude larger than the corresponding nematic values. Simulations carried out with either the mass or the moment of inertia of the molecules artificially set to infinity suggest that it is the freezing of the translational degrees of freedom which drives the transition.

We are grateful to Dr George Loriot for helpful discussions. Computational work in support of this research was performed at the Theoretical Physics Computing Facility at Brown University. This work was supported by the National Science Foundation under grant no. DMR-9217290 and DMR-9528092.

## References

[1] For experimental studies see, for example, (*a*) Speilberg, J. I., and Gelerinter, E., 1984, *Phys. Rev. B*, **32,** 3647; (*b*) Rosta, L., 1985, *Mol. Cryst. liq. Cryst.*, **127,** 195; (*c*) Dolganov, V. K., Fouret, R., Gors, C., and More, M., 1994, *Phys. Rev. E*, **49,** 5230.

[2] See, for example, (*a*) Villain, J., 1979, *Z. Phys. B*, **33,** 31; (*b*) Gabay, M., and Toulouse, G., 1981, *Phys. Rev. Lett.*, **47,** 201.

[3] Gay, J. G., and Berne, B. J., 1981, *J. chem. Phys.*, **74,** 3316.

[4] (*a*) DeMiguel, E., Rull, L. F., Chalam, M. K., and Gubbins, K. E., 1990, *Mol. Phys.*, **71,** 1223; (*b*) DeMiguel, E., Rull, L. F., Chalam, M. K., and Gubbins, K. E., 1991, *Mol. Phys.*, **74,** 405; (*c*) DeMiguel, E., Rull, L. F., and Gubbins, K. E., *Phys. Rev. A*, **45,** 3813.

[5] Luckhurst, G. R., Stephens, R. A., and Phippen, R. W., 1990, *Liq. Cryst.*, **8,** 451.

[6] Luckhurst, G. R., and Simmonds, P. S. J., 1993, *Mol. Phys.*, **80,** 233.

[7] DeMiguel, E., Rull, L. F., and Gubbins, K. E., 1992, *Phys. Rev. A*, **45,** 3813.

[8] (*a*) Sarman, S., and Evans, D. J., 1993, *J. chem. Phys.*, **99,** 620; (*b*) Sarman, S., 1994, *J. chem Phys.*, **101,** 480.

[9] Sarman, S., and Evans, D. J., 1993, *J. chem. Phys.*, **99,** 9021.

[10] Smondyrev, A. M., Loriot, G. B., and Pelcovits, R. A., 1995, *Phys. Rev. Lett.*, **75,** 2340.

[11] (*a*) Nose, S., 1984, *Mol. Phys.*, **52,** 255; (*b*) Hoover, W. G., 1985, *Phys. Rev. A*, **31,** 1695; (*c*) Nose, S., 1983, *Mol. Phys.*, **50,** 1055.

[12] Hashim, R., Luckhurst, G. R., and Romano, S., 1995, *J. chem. Soc. Faraday Trans.*, **91,** 2141.

[13] Edwards, S. F., and Anderson, P. W., 1975, *J. Phys. F*, **5,** 965.

[14] Nose, S., and Yonezawa, F., 1985, *Sol. State Commun.*, **56,** 1005.